ORIGINAL ARTICLE

Contribution of HCN1 variant to sinus bradycardia: A case report

Hangang Yu PhD[1] (ID) | Bryan Gall PhD[1] | Mackenzie Newman PhD[1] | Quincy Hathaway PhD[2] (ID) | Kathleen Brundage PhD[3] | Amanda Ammer PhD[3] | Peter Mathers PhD[4] | David Siderovski PhD[1] | Robert W. Hull MD[5]

[1]Department of Physiology and Pharmacology, School of Medicine, West Virginia University, Morgantown, WV, USA

[2]Department of Exercise Physiology, School of Medicine, West Virginia University, Morgantown, WV, USA

[3]Department of Microbiology, Immunology & Cell Biology, School of Medicine, West Virginia University, Morgantown, WV, USA

[4]Department of Neuroscience, School of Medicine, West Virginia University, Morgantown, WV, USA

[5]Department of Cardiology, School of Medicine, West Virginia University, Morgantown, WV, USA

Correspondence
Hangang Yu, Department of Physiology and Pharmacology, School of Medicine, West Virginia University, Morgantown, WV 26506, USA.
Email: hyu@hsc.wvu.edu

Present address
Bryan Gall, Variant Curator at Natera, San Carlos, CA, USA
David Siderovski, Pharmacology & Neuroscience, University of North Texas, Denton, TX, USA
Robert W. Hull, Department of Cardiology, Mon General Hospital, Morgantown, WV, USA

Abstract

Background: Missense mutations in the hyperpolarization-activated cyclic nucleotide-modulated (HCN) channel 4 (HCN4) are one of the genetic causes of cardiac sinus bradycardia.

Objective: To investigate possible HCN4 channel mutation in a young patient with profound sinus bradycardia.

Methods: Direct sequencing of *HCN4* and whole-exome sequencing were performed on DNA samples from the indexed patient (P), the patient's son (PS), and a family unrelated healthy long-distance running volunteer (V). Resting heart rate was 31 bpm for P, 67 bpm for PS, and 50 bpm for V. Immunoblots, flow cytometry, and immunocytofluorescence confocal imaging were used to study cellular distribution of channel variants. Patch-clamp electrophysiology was used to investigate the properties of mutant HCN1 channels.

Results: In P no missense mutations were found in the HCN4 gene; instead, we found two heterozygous variants in the HCN1 gene: deletion of an N-terminal glycine triplet (^{72}GGG^{74}, "N-del") and a novel missense variant, P851A, in the C-terminal region. N-del variant was found before and shared by PS. These two variations were not

found in V. Compared to wild type, N-del and P851A reduced cell surface expression and negatively shifted voltage-activation with slower activation kinetics.

Conclusion: Decreased channel activity HCN1 mutant channel makes it unable to contribute to early depolarization of sinus node action potential, thus likely a main cause of the profound sinus bradycardia in this patient.

KEYWORDS

HCN1, HCN4, hyperpolarization-activated ion channel, missense mutation, sinus bradycardia, whole-exome sequencing

1 | INTRODUCTION

Disease of the sinus node and resultant impairment of atrioventricular conduction induce an excessively low ventricular rate (bradycardia), which cannot meet the needs of the organism.[1] Sick sinus syndrome refers to intrinsic sinus node dysfunction that often results in symptomatic sinus bradycardia or sinus pauses.[1] In certain states, profound bradycardia can be associated with ventricular arrhythmias leading to cardiac arrest and sudden cardiac death.[2] Therefore, patients with sinus bradycardia in the absence of heart disease are often advised to implant an electronic pacemaker for preventing unexpected sudden cardiac death because of a lack of pharmaceutical options.[1]

The sinus node generates a spontaneous pacing action potential. The diastolic potential in the sinus node is around −65 mV.[3] HCN channels are highly expressed in the sinus node and are one of the main determinants in sinus node spontaneous pacemaker activity.[3] HCN channel activation is voltage-dependent.[4] HCN channel-generated inward current (also called cardiac pacemaker current, I_f) begins to activate around −45 to −50 mV in the sinus node[5,6] (defined as the threshold voltage of activation, V_{th}) and thus contributes to early diastolic depolarization in the sinus node.[6]

The HCN channel family has four members (HCN1-4).[7] In mammalian expression cell lines, HCN1 channels exhibit the most positive threshold voltage activation (−45 to −50 mV) associated with the fastest activation kinetics (~100 milliseconds near the threshold voltage activation), whereas HCN4 has the most negative threshold voltage activation (around −65 mV) associated with the slowest activation kinetics (~2000 milliseconds near the threshold voltage activation).[8,9]

The first HCN channel protein mutation linked to sinus bradycardia was HCN4-573x, reported in 2003.[10] So far, 30 HCN4 mutations have been identified in sinus bradycardia patients[11] and in patients with familial inappropriate sinus tachycardia,[12] Brugada syndrome,[13] ventricular fibrillation and left ventricular noncompaction,[14] left bundle branch block,[15] prolonged QT intervals, ST segment elevation, and *torsade de pointes* tachycardia,[4,16] as well as sudden infant death syndrome.[17] All HCN4 mutations are heterozygous. All loss-of-function mutations caused a reduced HCN pacemaker current via a negative shift of voltage-dependent activation[18] and/or decreased channel expression at the cell surface that reduces current density.[10,19,20] Both mechanisms cause HCN channels to produce a decreased inward current at diastolic depolarization, which reduces the sinus node spontaneous action potential and thus, slows the heart rate.

HCN4 transcript is most abundant in the sinus node of animals (mouse, rat, rabbit, canine) and humans.[21-25] However, recent studies of HCN channel protein expression levels have convincingly demonstrated that HCN1 protein levels are the highest followed by HCN4 in mouse[26] and human sinus node.[27] Mice lacking HCN1 developed severe sinus bradycardia and reduced cardiac output.[26] The ionic current (I_f encoded by HCN genes) that contributes to sinus node pacemaker activity is reduced by ~40%.[26]

Using both candidate gene and next-generation exome sequencing approaches, we report, for the first time, a novel missense variant in the HCN1 gene in a patient with profound sinus bradycardia, with the absence of missense mutations in HCN4, HCN2, and other voltage-gated ion channels (Nav1.5, Cav1.2, Cav1.3, Cav3.1) known to cause sinus bradycardia.

2 | METHODS (DETAILED METHODS ARE PROVIDED IN SUPPLEMENTAL MATERIALS)

2.1 | Human studies

The study protocol and blood drawing procedures were reviewed and approved by West Virginia University Institutional Review Board (IRB1508782471). Written consent forms were sufficiently explained in detail to, agreed, and signed by study participants.

2.2 | Electrocardiography of subjects

Heart rate was recorded by a standard 12-lead ECG from the patient (P), the patient's son (PS), and a family unrelated healthy volunteer (V).

2.3 | Genomic DNA isolation, HCN4 amplification, and direct sequencing

Genomic DNA was isolated from P, PS, and V using Qiagen DNA isolation kit for blood sample (QIAamp DNA Blood Mini Kit). HCN4 exons

were amplified using the primers specified in Table S1 and purified by gel electrophoresis. The WVU Genomic Core performed direct sequencing of HCN4 PCR products using sequencing primers described in Table S2.

2.4 | Whole-exome sequencing and variation analysis

Whole-exome sequencing was performed on genomic DNA samples from P, PS, and V by Applied Biological Materials Inc (ABM). Variation-call-format (VCF) files were generated by ABM, then visualized and analyzed using Integrative Genomic Viewer[28] and gnomAD[29] for missense variations.

2.5 | GFP-tagged HCN1 mutant constructs

Wild-type human HCN1 (WT or wtHCN1) in pcDNA3 was used for the construction of variants for [72]GGG[74] and P851A. wtHCN1 and mutants were then cloned into the N-terminus of pEGFP-C1 mammalian expression vector.

2.6 | Cell culture and transfection

Human embryonic kidney (HEK293) cells were used for the expression of wild-type and mutant HCN1 channels. Transient plasmid transfection was performed using Lipofectamine_3000 (Invitrogen) following the vendor's instructions.

2.7 | Western blotting

HEK293 cells transfected with wtHCN1 and mutant channel plasmids were harvested in RIPA buffer with fresh protease and phosphatase inhibitor cocktail (Sigma) on ice using a cell scraper. Detailed procedures are similar to our previous report[9] and are provided in Data Supplements.

2.8 | Flow cytometry

HEK293 cells expressing wtHCN1 and mutants were harvested 2 days after transfection using 0.25% trypsin with EDTA. Samples were analyzed in the WVU Flow Cytometry & Single Cell Core Facility on a four laser BD LSRFortessa. Details are provided in Data Supplements.

2.9 | Confocal imaging of HEK293 cells expressing HCN1 mutant channels

HEK293 cells transfected with wild-type and mutant HCN1 channels were incubated on coverslips and fixed in 4% paraformaldehyde/

PBS. The cells were imaged by the Nikon Sweptfield Confocal microscopy.

2.10 | Whole-cell patch-clamp electrophysiology studies

Whole cell patch-clamp studies were carried out in HEK293 cells at 35-37°C. Details of patch-clamp studies are similar to our previous reports[9,30] and are provided in Data Supplements.

Threshold voltage (V_{th}) for HCN channel activation was defined as the least negative voltage at which HCN channels begin to open, generating a time-dependent inward current of at least 10pA was observed detected (a value that allowed clear discrimination from background noise, as seen in our previous publication[31]).

2.11 | Sinoatrial pacemaker activity cell model

OpenCOR 0.1 software[32] was used to simulate the effect of HCN1 variant changes in sinoatrial pacemaker activity using an updated sinoatrial pacemaker activity cell model.[33]

2.12 | Statistical analysis

Statistical analyses were performed by one-way ANOVA followed by post hoc test Bonferroni (all means compared to wtHCN1) or Tukey (multiple comparisons with each other). The averaged data were presented as means ± SD. A P-value of less than.05 was considered as statistically significant.

3 | RESULTS

3.1 | Patient studies

The patient, a 42-year-old African American, was not on any medication nor had electrolyte abnormalities. Despite no evidence of structural heart disease by echocardiography, a 12-lead EKG showed profound symptomatic sinus bradycardia in his 30s. His mother had been previously diagnosed with sick sinus syndrome and underwent pacemaker implantation. The patient received a dual-chamber pacemaker and experienced complete relief of symptoms.

The patient's son was a healthy teenage boy (age 15 years), and a family unrelated healthy volunteer (male, 26 years) who is an amateur long-distance runner, served as a volunteer control. Resting heart rate was obtained from a 12-lead electrocardiograph (ECG) for P (Figure 1A, HR = 31 bpm, with complete heart block), PS (Figure 1B, HR = 67 bpm), and V (Figure 1C, HR = 50 bpm).

3.2 | Direct sequencing of HCN4 gene

Previous studies have established HCN4 mutations as one of the genetic causes in patients with sinus bradycardia. HCN4 gene contains 8 exons.[10,34] We used amplification primers (Table S1) to obtain each exon from genomic PCR and subsequent gel electrophoresis, and sequencing primers (Table S2) to sequence the HCN4 gene. We found no missense mutations in HCN4 gene from the patient, the son, and the volunteer.

3.3 | Exome-sequencing discovery of HCN1 variants in the patient

To explore a comprehensive genetic cause of the patient's bradycardia, we performed next-generation exome sequencing on genomic DNA isolated from P, PS, and V. In HCN4 gene, we found no missense variant, but did find one known heterozygous synonymous variant (rs529004) in the C-terminal region, shared by PS and V (Figure 2A). In HCN2 gene (another HCN isoform expressed at a very low level compared to HCN1 and HCN4 in the sinus node[21,24]), we found no missense, but five known heterozygous synonymous variations (rs55659726, rs56170955, rs55780677, rs12981860, rs1054786).

In HCN1, two variants were found in the patient. One is located in the N-terminus in HCN1 exon_1, *rs55852304 (now merged into* rs560604803), located in *Human hg19*: Chr5: 45695986-45695995. It is an in-frame deletion (indel), *GCCGCCGCC*, which encodes $^{72}GGG^{74}$ in the protein sequence (HGVS nomenclature: NM_021072.3:c. 187_195delGGCGGTGGC). This $^{72}GGG^{74}$ deletion is found in three gene variant databases mentioned above and is shared by the patient's son (Figure 2B). This allele frequency in global population according to 1000Genomes is 2.2% (https://www.ncbi.nlm.nih.gov/snp/rs56064803#frequency_tab).

A missense c.2551C>G transversion variant was found in *Human hg19*: Chr5: 45262145, in exon8 of HCN1, causing a p. Pro851Ala [CCC (Pro) → GCC(Ala)] missense mutation (Figure 2C). The protein and nucleotide sequences alignments are shown in Figure S1 and S2). This variant is not found in (1) National Heart, Lung, Blood Institute (NHLBI) GO Exome Sequencing Project (ESP) [Exome Variant Server, NHLBI GO Exome Sequencing Project (ESP), Seattle, WA (http://evs.gs.washington.edu/EVS/) [accessed: Jan 11, 2019], containing 6403 samples; (2) Exome Aggregation Consortium (ExAC) (which has about 60 000 individuals) (http://exac.broadinstitute.org/) [accessed: Jan 11, 2019]; and (3) the genome Aggregation Database (gnomAD, an upgraded version of ExAC, covering two datasets: exome sequence data from 123 136 individuals and whole genome sequencing from 15 496 individuals, https://gnomad.broadinstitute.org/gene/ENSG00000164588) [accessed: Jan 12, 2019] (Figure S3). To our best knowledge, P851A is a novel variant that has not been reported before in bradycardia patient.

Sequencing alignment across species on MARRVEL[35] indicated that P851 is conserved in the polypeptide sequence of HCN1 of human (hs, *Homo sapiens*), mouse (mm1, *Mus musculus*), rat (rn1, *Rattus norvegicus*), Zebrafish (dr1, *Danio rerio*), and Fly (dm1, *Drosophila melanogaster*) (arrows in Figure S4). PolyPhen-2[36] predicted that P851A variant is "probably damaging" with a score of 0.999. The Sorting Intolerant From Tolerant (SIFT) algorithm predicts the effects of a missense variant on protein function.[37,38] SIFT predicted that P851A is not tolerated (Supplemental excel file HCN1 SIFT, row 62, highlighted).

Missense mutations in the voltage-dependent calcium (Cav1.2, Cav1.3, Cav3.1) and sodium (Nav1.5) channels have been reported to be linked to bradycardia.[39-42] We found no missense mutations in these channel genes SCN5A (Nav1.5), CACNA1C (Cav1.2), CACNA1D (Cav1.3), CACNA1G (Cav3.1, T-type) from the patient. We have also studied sequences of other genes associated with bradycardia (KCNK17, RYR2, CASQ2, AMK2, MYH6),[43] and found no missense mutations.

From VCF (variant call format) files, the patient was heterozygous for N-del and P851A. The patient's son has the N-del but not the P851A. Although additional blood samples from the patient's parents and siblings were unavailable, it is almost certain that the two mutations are on different alleles, otherwise, the son would inherit both or neither. Thus, we studied co-expression of N-del + P851A (mimic the patient's variant) and N-del + wtHCN1 (mimic the son's variant).

3.4 | Protein expression of HCN1 mutants

We first examined the surface expression of HCN1 mutants transfected into HEK293 cells. In membrane preparations, a human HCN1
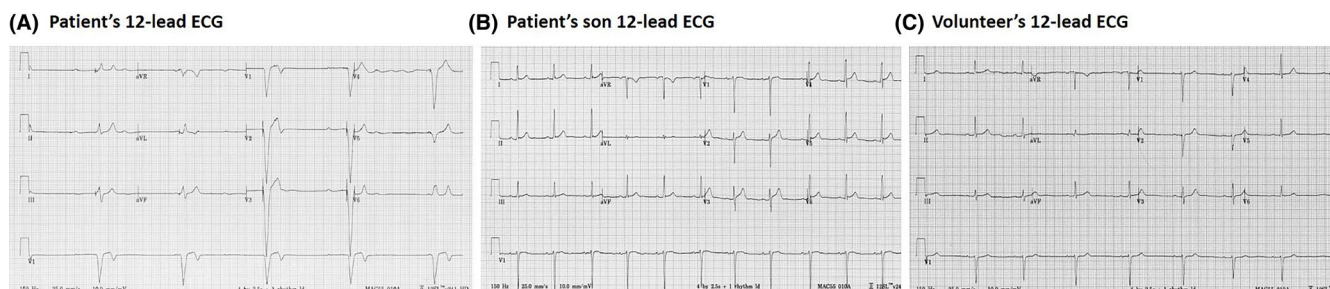

FIGURE 1 12-lead ECG recordings. (A) Index patient (resting heart rate was 31 bpm). (B) Patient's son (resting heart rate was 67 bpm). (C) Volunteer (resting heart rate was 50 bpm)
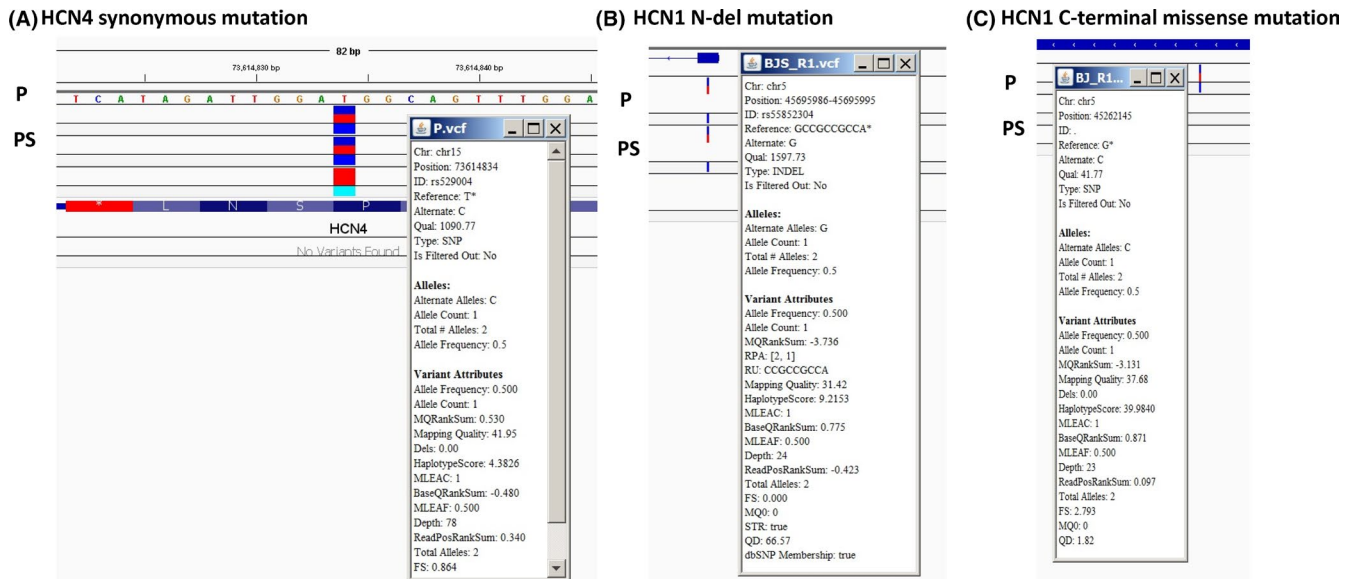
FIGURE 2 HCN4 and HCN1 gene mutations viewed in IVG. (A) HCN4 synonymous mutations. (B) HCN1 N-del mutation. (C) HCN1 C-terminal missense mutation. P, patient, PS, patient's son

FIGURE 3 Western blots of HCN1 mutants in HEK293. In cell membrane preparation (left), immunoblots are shown for WT, P851A, and N-del channel proteins (A) and for N-del + wtHCN1, N-del + P851A, and wtHCN1wt channel proteins (B). (C) Average surface channel protein expression of WT, N-del, N-del + P851A, P851A, and N-del + wtHCN1, normalized to β-actin. In total cell lysate (right), immunoblots are shown for WT, P851A, and N-del channel proteins (D) and for N-del + wtHCN1, N-del + P851A, and wtHCN1wt channel proteins (E). (H) Average total channel protein expression of WT, N-del, N-del + P851A, P851A, and N-del + wtHCN1, normalized to β-actin
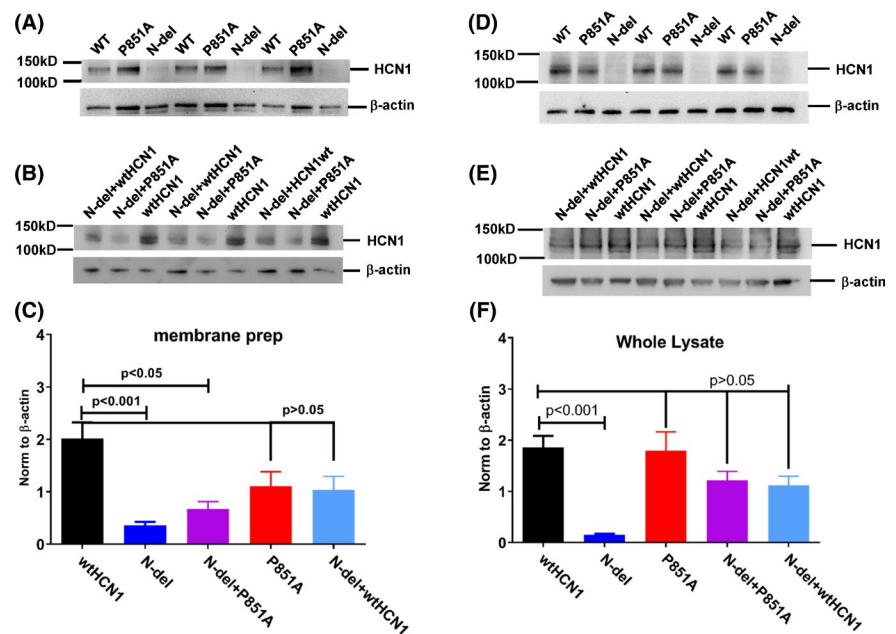
antibody detected protein expression of WT, N-del, and P851A HCN1 channels at the expected molecular weight (~120 kDa) (Figure 3A). Co-expression of wide-type HCN1 with the mutant channels (N-del + wtHCN1 for PS, N-del + P851A for P) are shown in Figure 3B.

On average, there was over five-fold reduction in surface expression of N-del, compared to the wild-type HCN1 channel protein, after being normalized to the loading control (Figure 3C) (WT: 2.01 ± 0.830, n = 7; N-del: 0.36 ± 0.17; n = 6, $P < .001$). There was a three-fold reduction of surface expression in N-del + P851A compared to the wildtype channel (WT: 2.01 ± 0.830, n = 7; N-del + P851A: 0.67 ± 0.28; n = 4, $P < .01$). There was no statistical difference in surface expression levels of P851A comparing to the wildtype channels (WT: 2.01 ± 0.830,

n = 7; P851A: 1.11 ± 0.55; n = 4, $P > .05$) and N-del + wtHCN1 (WT: 2.01 ± 0.830, n = 7; N-del + wtHCN1: 1.04 ± 0.44; n = 4, $P > .05$) channel proteins (Figure 3C).

Total channel protein levels were examined in the whole lysate preparations. N-del (Figure 3D) and N-del + P851A (Figure 3E) showed a reduction in channel protein levels compared to wild-type HCN1. The channel protein levels are decreased by ~12-fold for N-del in comparison to the WT, while changes in P851A, N-del + P851A, and N-del + wtHCN1 were statistically not significant (Figure 3F) (WT: 1.86 ± 0.56, n = 6; N-del: 0.15 ± 0.04, n = 6; P851A: 1.80 ± 0.81, n = 5; N-del + P851A: 1.21 ± 0.44, n = 6; N-del + HCN1wt: 1.12 ± 0.40, n = 5).

Additionally, we used flow cytometry to detect the surface expression of channel proteins at the single cell level. A hemagglutinin (HA) tag in the extracellular loop between S3 and S4 transmembrane domains was introduced into the HCN1 wild-type and mutant constructs (WT, P851A, N-del). We used an HA-antibody conjugated with Alexa647 to stain surface expression of HCN1 mutants in cells without permeabilization. For intracellular staining, we used an HCN1-antibody conjugated with phycoerythrin (PE) fluorophore after cells were permeabilized. The HCN1 antibody targets an intracellular epitope (amino acid residues 790-883) in the C terminus of the protein (Thermo Scientific, PA553950). GFP-positive cells that bind to HA-APC antibody prior to permeabilization were counted (Figure 4A). The fluorescent signals are contributed by HA-tagged HCN1 channels expressing at the cell surface. The total number of channels at cell surface is the product of the count and the median or geometric mean of HA-APC fluorescent signals (Figure 4B). Surface expression of N-del + wtHCN1 channels are decreased by 69% when normalized to WT (WT: 1, N-del + wtHCN1: 0.31 ± 0.09; n = 5, $P <$ 001). Expression levels of N-del + P851A channels at cell surface are also decreased, but to lesser extent, 24% (WT: 1; N-del + P851A: 0.76 ± 0.11; $P <$ .01, n = 5). There is no statistical difference between the surface expression levels of P851A and WT HCN1 channels (WT: 1; P851A: 0.92 ± 0.17; $P >$ .05, n = 5). Figure S5 shows that surface expression of N-del channels is decreased by 71% (WT: 1; N-del: 0.29 ± 0.11; $P <$ .001, n = 5), but the surface expression of P851 channels is not statistically different from wild-type channel (WT: 1; P851A: 0.87 ± 0.31; $P >$ .05, n = 5).

3.5 | Confocal imaging studies of HCN1 mutants

We also performed confocal imaging studies of HCN1 mutant channels co-expressed with the wild-type HCN1 in HEK293 cells. Representative channel distributions (green) are shown for the volunteer (wtHCN1) (Figure 4C), the patient (N-del + P851A) (Figure 4D), and the patient's son (wtHCN1 + N-del) (Figure 4E). The relative channel distribution was estimated by calculating the total number of the expressed channels divided by the total cell area from the brightfield image, the averaged results are shown in Figure 4F. Compared to the wild-type HCN1, the total number of channels was >fivefold decreased for wtHCN1 + P851A and >3-fold decreased for wtHCN1 + N-del (wtHCN1: 0.54 ± 0.20, N-del + wtHCN1: 0.16 ± 0.02, N-del + P851A: 0.095 ± 0.079, n = 6, $P <$ .05). There was no significant difference in the average ratio of GFP area to total cell area between N-del + P851A and N-del + wtHCN1 using one-way ANOVA followed by post hoc test Tukey (N-del + wtHCN1: 0.155 ± 0.0593, N-del + P851A: 0.0958 ± 0.0884, $P >$ .05) (Figure 4F).

3.6 | Biophysical properties of HCN1 mutants

Studies of HCN4 mutations have revealed two mechanisms by which missense mutations cause reduced channel activity: reduced channel expression and/or a negative shift of voltage-dependent activation.[18] Therefore, we investigated the threshold activation (the least negative potential at which the HCN channel inward current of 10pA can be detected[31]) and the current density (the whole-cell current
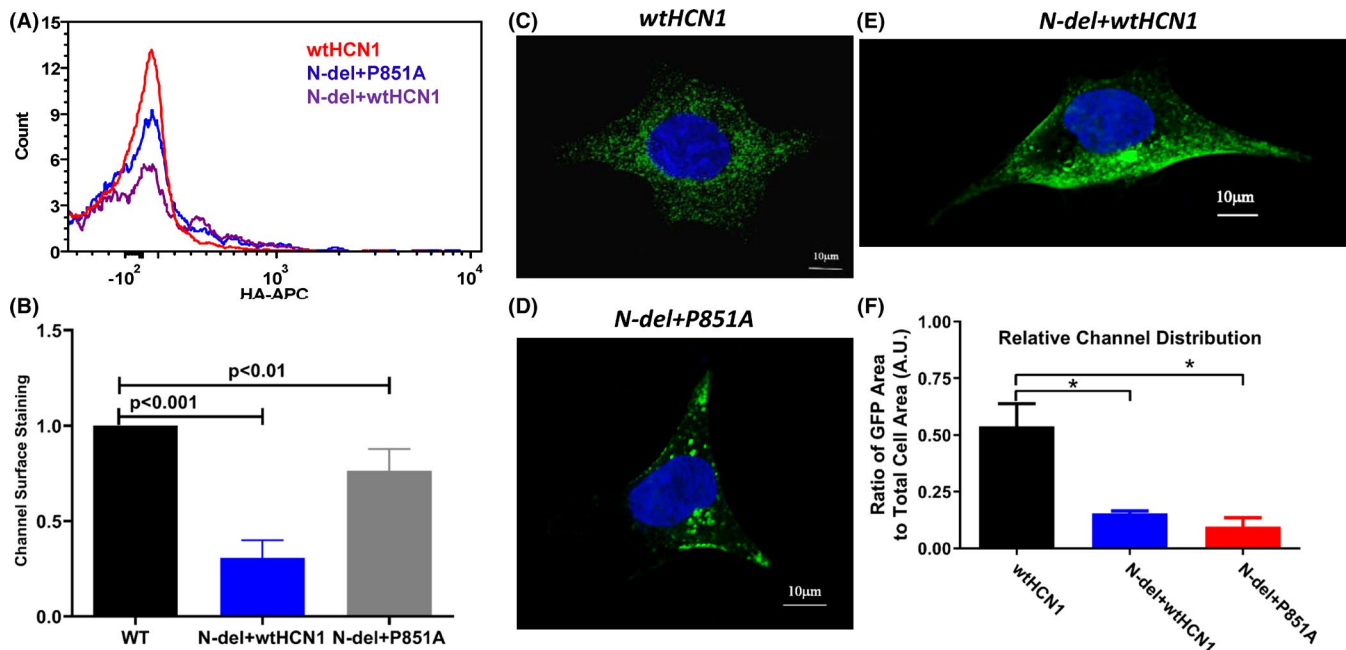
FIGURE 4 Flow cytometry and confocal imaging studies of HCN1 mutant channel surface expression. Representative flow experiments for surface staining of wtHCN1, N-del + wtHCN1, and N-del + P851A. (B) Averaged percentage of channel surface staining of wtHCN1, N-del + wtHCN1, and N-del + P851A, normalized to wild-type HCN1. An HA-APC antibody was used to recognize the HA-tag in the channel constructs. (C) Confocal images of wtHCN1, (D) N-del + P851A, (E) N-del + wtHCN1. (F) Average ratio of GFP area (representing number of channels) to the total cell area. * indicates statistical significance ($P <$ .05)
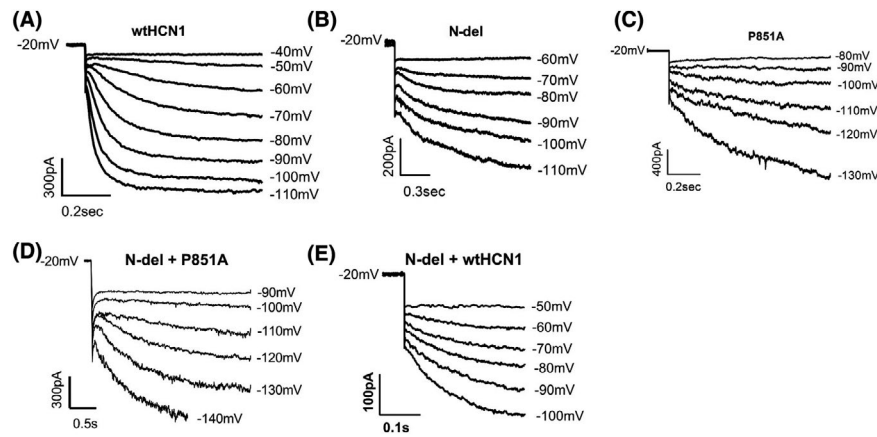
FIGURE 5 Biophysical properties of HCN1 mutant channels. (A) Wild-type channel currents were elicited by 1-s hyperpolarizing pulses from −40 to −110 mV in 10 mV increments. (B) N-del channel currents were elicited by 1.5s hyperpolarizing pulses from −60 to −110 mV in 10 mV increments. (C) P851A channel currents were elicited by 1s hyperpolarizing pulses from −80 to −130 mV in 10 mV increments. (D) N-del + P851A channel currents were elicited by 3.5s hyperpolarizing pulses from −90 to −140 mV in 10 mV increments. (E) N-del + wtHCN1 channel currents were elicited by 1s hyperpolarizing pulses from −50 to −100 mV in 10 mV increments. The holding potential was −20 mV for all cells studied

divided by cell capacitance), which reflects the functional channels of HCN1 mutants available at the cell surface.

Figure 5 shows the representative current activation of wild-type human version HCN1 (wt-hHCN1) and the mutant channels expressed in HEK293 cells. Channel-expressing cells were voltage-clamped at −20 mV and hyperpolarized to a range of potentials marked in the figure. Compared to wild-type HCN1 (Figure 5A), N-del (Figure 5B), P851A (Figure 5C), N-del + P851A (Figure 5D), and N-del + wtHCN1 (Figure 5F) mutant channels were activated at more negative potentials. The average threshold activation is −52.0 ± 3.3 mV (n = 7) for WT, −65.0 ± 7.1 mV (n = 10) for P851A, −67.5 ± 4.5 mV (n = 10) for N-del, −68.8 ± 8.3 mV (n = 7) for N-del + wtHCN1, and −107.5 ± 12.2 mV (n = 12) for N-del + P851A, respectively (Figure 6A). There exists a statistically significant negative shift in the threshold activation for P851A (−13 mV), for N-del (−15 mV), for N-del + wtHCN1 (−16 mV), and for N-del + P851A (−55 mV), respectively, when compared to the wild-type HCN1 (Table 1). There was a significance difference of HCN1 mutant channel threshold activation between N-del + P851A and N-del + wtHCN1 using one-way ANOVA followed by post hoc test Tukey (N-del + wtHCN1: −68.75 ± 8.35 mV, N-del + P851A: −107.5 ± 12.15 mV, $P < .05$) (Figure 6A).

The half-voltage activation of mutant channels is also significantly shifted to hyperpolarizing potentials compared to wild-type

(Table 1): N-del by −19 mV, P851A by −23 mV, N-del + P851A by −49 mV, and N-del + HCN1wt by −12 mV, respectively. Wild-type HCN1 channel has fast activation kinetics (100-300 milliseconds near threshold voltage of activation).[8,44] All mutant channels have slower activation kinetics near their respective threshold voltage of activation (τ_{Vth}) (Table 1), notably, N-del + P851A has the slowest activation kinetics near the voltage threshold of activation.

We next measured the current density (current amplitude normalized to the cell capacitance, pA/pF) of HCN1 mutant channels at the voltage where the channels are fully activated to calculate the relative functional channels available at the cell surface. Compared to WT, there is a 47% reduction of current density for N-del (WT (−110 mV): 27.3 ± 2.0 pA/pF, n = 5; N-del (−130 mV): 14.4 ± 2.7 pA/pF, n = 7), a 51% reduction of current density for N-del + P851A (WT (−110 mV): 27.3 ± 2.0 pA/pF, n = 5; N-del + P851A (−140 mV): 13.5 ± 3.4 pA/pF, n = 7), and a 44% decrease in current density for N-del + HCN1wt (WT (−110 mV): 27.3 ± 2.0 pA/pF, n = 5; N-del + HCN1wt (−110 mV): 15.3 ± 3.3 pA/pF, n = 5). On the other hand, P851A showed no statistical decrease in current density compared to WT HCN1 channels (WT (−110 mV): 27.3 ± 2.0 pA/pF, n = 7; P851A (−130 mV): 21.6 ± 1.9 pA/pF, $P > .05$, n = 8) (6B, Table 1). There was no significance difference of HCN1 mutant channel current density between N-del + P851A and N-del + wtHCN1 using one-way ANOVA followed by post hoc test Tukey (N-del + wtHCN1:
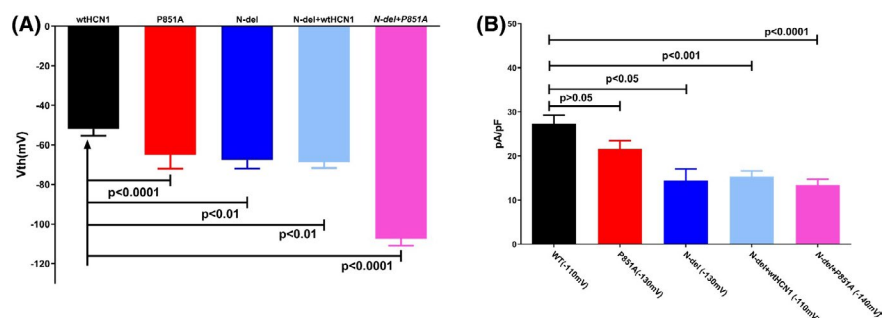
FIGURE 6 Average HCN1 mutant channel threshold activation (A) and current density (B)

TABLE 1 HCN1 mutant properties

	WT	N-del	P851A	N-del + P851A	N-del + HCN1wt
V_{th} (mV)	−52.0 ± 3.3 (n = 7)	−67.5 ± 4.5* (n = 10)	−65.0 ± 7.1*** (n = 10)	−107.5 ± 12.2*** (n = 12)	−68.8 ± 8.3** (n = 7)
V_{50} (mV)	−68.8 ± 2.3 (n = 6)	−87.70 ± 4.6** (n = 7)	−91.56 ± 3.7** (n = 7)	−118.30 ± 15.1*** (n = 8)	−81.1 ± 7.6* (n = 5)
τV_{th} (ms)	98.3 ± 38.2 (n = 7)	468.1 ± 79.5** (n = 10)	353.4 ± 50.7** (n = 10)	925.2 ± 311.8* (n = 8)	124.8 ± 30.8 (n = 6)
pA/pF (max. mV)	27.3 ± 2.0 (−110 mV) (n = 5)	14.4 ± 2.7* (−130 mV) (n = 6)	21.6 ± 1.9 (−130 mV) (n = 6)	13.5 ± 3.4*** (−140 mV) (n = 7)	15.3 ± 3.3*** (−110 mV) (n = 5)

*$P < .05$ compared to WT; **$P < .01$ compared to WT; ***$P < .001$ compared to WT.

15.33 ± 3.33 pA/pF, N-del + P851A: 13.47 ± 3.39 pA/pF, $P > .05$) (Figure 6B).

One of the hallmarks of HCN channels is the functional channel blockade by ZD7288, a selective blocker for HCN pacemaker channels.[45] Figure 7 shows the ionic current inhibition of HCN1 wild-type (A), mutant channels (B, N-del; C, P851A), co-expression of N-del and P851A (D), and co-expression of N-del with wild-type channel (E) by 10 μM ZD7288 at the respective membrane potential.

3.7 | Effect of HCN1 variant in the sinoatrial pacemaker activity

To evaluate the effect of HCN1 variant in the sinoatrial pacemaker activity, we employed an updated sinoatrial pacemaker activity cell model developed by DiFrancesco's group.[33] HCN1 protein levels are >15-fold higher than HCN4 and HCN2 in the sinus node.[27] We assumed that removing the main contributor HCN1 result in one-third decrease in I(f) channel conductance; the simulation result showed that the rate of spontaneous action potential is decreased by about 50% because of reduction in the initial phase 4 depolarization speed (control: ~110 mV/s, HCN1 variant: ~60 mV/s) (Figure 8, A-control action potential (upper) and I(f) (lower), B-reduced rate of action potential (upper) and I(f) (lower)).

4 | DISCUSSION

In the index patient, both direct- and exome-sequencing revealed no missense mutations in HCN4; instead, we found two variants in the HCN1 gene. One variant is an indel located in the N-terminus ([72]GGG[74]) and the other is P851A located in the C-terminus. The [72]GGG[74] N-del is found in the National Heart, Lung, Blood Institute GO Exome Sequencing Project database [Exome Variant Server, NHLBI GO Exome Sequencing Project (ESP), Seattle, WA (URL: http://evs.gs.washington.edu/EVS/)].

Currently, 29 variations in HCN1 gene have been found in patients with epilepsy.[46] Four (T171R in the S1-S2 loop, C329S in the S5-S6 loop, V414M and S680Y in the C-terminus) are characterized as inherited, likely pathogenic variations, nineteen are novel pathogenic variants, and the rest are of unknown clinical significance. N-del ([72]GGG[74] indel, p. Gly72_Gly74del, or c.187_195del) was previously found in idiopathic generalized epilepsy (rs56064803)[47] and in an early infantile epileptic encephalopathy patient, but its clinical significance has been characterized as benign using a Sherloc criteria[48] (National Center for Biotechnology Information. ClinVar; Variation ID 95999, https://preview.ncbi.nlm.nih.gov/clinvar/variation/95999/ (accessed Feb. 24, 2019)). To our best knowledge, this is the first time that a patient exhibiting the rs56064803 indel with profound sinus bradycardia has presented with absence of epilepsy.

P851A (c.2551C>G) is not found in NHLBI GO exome and gnomAD databases and has not been previously reported in the

FIGURE 7 ZD7288 blockade of HCN1 mutant channel activation. The channel current is shown in black and ZD7288 (10 μM) in gray line. ZD7288 blocked wild-type HCN1 channel current at −90 mV (A), N-del channel current at −110 mV (B), P851A channel current at −130 mV (C). N-del + P851A channel current at −120 mV (D), and N-del + wtHCN1 at −100 mV (E). The holding potential was −20mV for all cells studied
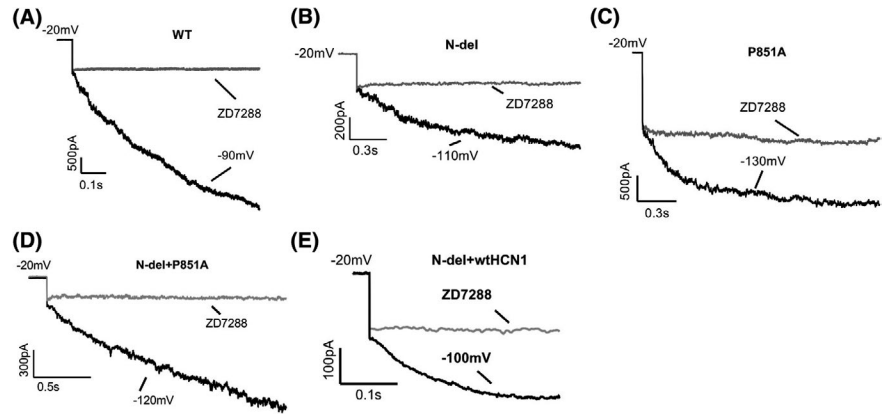
FIGURE 8 Effect of HCN1 variants on sinoatrial pacemaker activity. (A) Control action potential (upper) and *I*(f) current (lower). (B) Effects of a decreased *I*(f) channel conductance by 33% on action potential (upper) and *I*(f) current (lower). Vertical dotted line: *I*(f) current amplitude
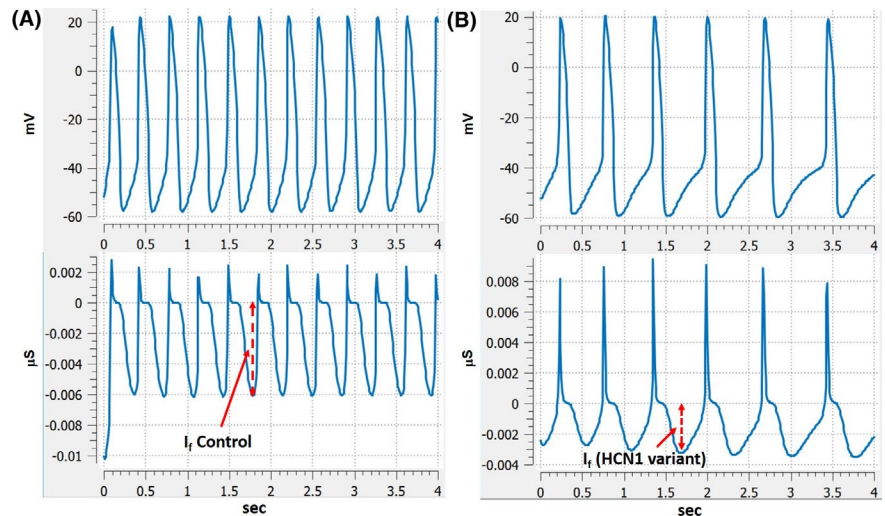
literature. Therefore, we consider it a de novo missense variant in HCN1 gene. Protein expression studies using immunoblots, confocal imaging, and flow cytometry indicated that N-del is defective in biosynthesis, resulting in reduced channel expression at the cell surface. On the other hand, P851A does not exhibit a significant change in channel surface expression compared to the wild-type channels.

Co-expression of N-del with P851A also showed decreased cell surface expression of the channels, although the total protein synthesis was not statistically reduced compared to the wild-type channel. Decreased surface expression of co-expressed N-del with wild-type HCN1 (patient's son situation) was not detected by immunoblots, but by confocal imaging and flow cytometry. Importantly, the decreased number of functional channels of N-del + wtHCN1 were reflected in patch-clamp studies as significantly reduced current density.

Alterations in voltage-dependent activation of the mutant channels are of direct relevance to the inward current contributed to the early diastolic depolarization phase in sinus node action potential. Both N-del and P851A have a negative shift in the threshold voltage activation associated with a simultaneous, significant slowing of activation kinetics, compared to the wild-type HCN1.

The compound variant, N-del + P851A, has the largest hyperpolarizing shift in the threshold voltage activation versus N-del and P851A. Additionally, among the three HCN channel isoforms present in the sinus node, HCN1 has the fastest activation kinetics during the diastolic phase, comparable to pacemaker current activation kinetics in the sinus node (~1s).[49] A combination of negative shift of voltage-dependent activation and a significantly slowed activation kinetics make the compound mutant (N-del + P851A) channel unable to contribute to the diastolic depolarization of the sinus node. This channel gating mechanism also explains why the patient's son is asymptomatic: although surface expression of N-del + wtHCN1 is reduced, the channel activities (V_{th}, $V_{1/2}$, and τ_{th}) are not suppressed to the extent seen in the compound variant (N-del + P851A).

To further understand how the compound mutant (N-del + P851A) affects the heart rate in the patient, we performed a simulation of sinoatrial pacemaker activity affected by HCN1 variant. The simulation result demonstrated that removal of HCN1 contribution to overall pacemaker current significantly decreased pacemaker channel conductance, resulting in a decreased phase-4 depolarization and a nearly 50% reduction in the pacemaker activity, which mimics the profound bradycardia in the indexed patient.

5 | CONCLUSIONS

In the present work, we report two HCN1 variants found in the indexed bradycardia patient, in the absence of missense mutations of HCN4 and other channels known to cause cardiac bradycardia. Our data indicated that N-del HCN1 has defective protein biosynthesis, but unlikely contributes to the patient's bradycardia since it is shared by his son who does not have bradycardia. The novel P851A variant does not have reduced channel expression at cell surface but exhibits a negative shift of voltage-dependent activation. The combination of two variants, N-del + P851A (present only in the patient), has the largest negative shift of voltage-dependent activation of HCN1 channels beyond the early diastolic depolarization of sinus node, which represents the likely cause of profound sinus bradycardia in the patient in the absence of missense variants in other ion channels previously linked to sinus bradycardia.

CONFLICT OF INTEREST

Authors declare no conflict of interest for this article.

ORCID

Hangang Yu https://orcid.org/0000-0001-6838-8310
Quincy Hathaway https://orcid.org/0000-0001-8226-2319

REFERENCES

1. Adan V, Crown LA. Diagnosis and treatment of sick sinus syndrome. Am Fam Physician. 2003;67:1725–32.
2. Adabag AS, Luepker RV, Roger VL, Gersh BJ. Sudden cardiac death: epidemiology and risk factors. Nat Rev Cardiol. 2010;7:216–25.
3. Baruscotti M, Difrancesco D. Pacemaker channels. Ann N Y Acad Sci. 2004;1015(1):111–21.
4. Herrmann S, Hofmann F, Stieber J, Ludwig A. HCN channels in the heart: lessons from mouse mutants. Br J Pharmacol. 2012;166(2):501–9.
5. Wu JY, Yu H, Cohen IS. Epidermal growth factor increases I(f) in rabbit SA node cells by activating a tyrosine kinase. Biochem Biophys Acta 2000;1463:15–9.
6. DiFrancesco D. Pacemaker mechanisms in cardiac tissue. Annu Rev Physiol. 1993;55:455–72.
7. Santoro B, Tibbs GR. The HCN gene family: molecular basis of the hyperpolarization-activated pacemaker channels. Ann N Y Acad Sci. 1999;868:741–64.
8. Biel M, Schneider A, Wahl C. Cardiac HCN channels: structure, function, and modulation. Trends Cardiovasc Med 2002;12(5):206–13.
9. Lin Y-C, Huang J, Kan H, Frisbee JC, Yu H-G. Rescue of a trafficking defective human pacemaker channel via a novel mechanism: roles of Src, Fyn, Yes tyrosine kinases. J Biol Chem. 2009;284:30433–40.
10. Schulze-Bahr E, Neu A, Friederich P, Kaupp UB, Breithardt G, Pongs O, et al. Pacemaker channel dysfunction in a patient with sinus node disease. J Clin Invest. 2003;111(10):1537–45.
11. Verkerk AO, Wilders R. Pacemaker activity of the human sinoatrial node: an update on the effects of mutations in HCN4 on the hyperpolarization-activated current. Int J Mol Sci. 2015;16:3071–94.
12. Barbuti A, Bucchi A, Paina M, Milanesi R, DiFrancesco D, Baruscotti M, et al. A gain-of-function mutation in the cardiac pacemaker HCN4 channel increasing cAMP sensitivity is associated with familial Inappropriate Sinus Tachycardia. Eur Heart J. 2015;38:280–88.
13. Biel S, Aquila M, Hertel B, Berthold A, Neumann T, DiFrancesco D, et al. Mutation in S6 domain of HCN4 channel in patient with suspected Brugada syndrome modifies channel function. Pflugers Archiv: Eur J Physiol. 2016;468(10):1663–71.
14. Servatius H, Porro A, Pless SA, et al. Phenotypic spectrum of HCN4 mutations: a clinical case. Circ Genom Precis Med. 2018;11:e002033.
15. Yokoyama R, Kinoshita K, Hata Y, Abe M, Matsuoka K, Hirono K, et al. A mutant HCN4 channel in a family with bradycardia, left bundle branch block, and left ventricular noncompaction. Heart Vessels. 2018;33(7):802–19.
16. Herrmann S, Stieber J, Ludwig A. Pathophysiology of HCN channels. Pflügers Archiv - Eur J Physiol. 2007;454(4):517–22.
17. Evans A, Bagnall RD, Duflou J, Semsarian C. Postmortem review and genetic analysis in sudden infant death syndrome: an 11-year review. Human Pathol. 2013;44(9):1730–6.
18. Milanesi R, Baruscotti M, Gnecchi-Ruscone T, DiFrancesco D. Familial sinus bradycardia associated with a mutation in the cardiac pacemaker channel. N Engl J Med. 2006;354:151–7.
19. Nof E, Luria D, Brass D, Marek D, Lahat H, Reznik-Wolf H, et al. Point mutation in the HCN4 cardiac ion channel pore affecting synthesis, trafficking, and functional expression is associated with familial asymptomatic sinus bradycardia. Circulation. 2007;116:463–70.
20. Ueda K, Nakamura K, Hayashi T, Inagaki N, Takahashi M, Arimura T, et al. Functional characterization of a trafficking-defective HCN4 mutation, D553N, associated with cardiac arrhythmia. J Biol Chem. 2004;279:27194–8.
21. Shi W, Wymore R, Yu H, Wu J, Wymore RT, Pan Z, et al. Distribution and prevalence of hyperpolarization-activated cation channel (HCN) mRNA expression in cardiac tissues. Circ Res. 1999;85:e1–6.
22. Shi W, Yu H, Wu J, Zuckerman J, Wymore R, Dixon JE, et al. The distribution and prevalence of HCN isoforms in the canine heart and their relation to the voltage dependence of I_f. Biophys J. 2000;78:353A.
23. Herrmann S, Layh B, Ludwig A. Novel insights into the distribution of cardiac HCN channels: an expression study in the mouse heart. J Mol Cell Cardiol. 2011;51:997–1006.
24. Chandler NJ, Greener ID, Tellez JO, Inada S, Musa H, Molenaar P, et al. Molecular architecture of the human sinus node: insights into the function of the cardiac pacemaker. Circulation. 2009;119:1562–75.
25. Brioschi C, Micheloni S, Tellez JO, Pisoni G, Longhi R, Moroni P, et al. Distribution of the pacemaker HCN4 channel mRNA and protein in the rabbit sinoatrial node. J Mol Cell Cardiol. 2009;47(2):221–7.
26. Fenske S, Krause SC, Hassan SIH, Becirovic E, Auer F, Bernard R, et al. Sick sinus syndrome in HCN1-deficient mice. Circulation. 2013;128:2585–94.

27. Li N, Csepe TA, Hansen BJ, Dobrzynski H, Higgins RS, Kilic A, et al. Molecular mapping of sinoatrial node HCN channel expression in the human heart. Circ Arrhythm Electrophysiol 2015;8(5):1219–27.

28. Robinson JT, Thorvaldsdóttir H, Winckler W, Guttman M, Lander ES, Getz G, et al. Integrative genomics viewer. Nat Biotechnol. 2011;29(1):24–6.

29. Karczewski KJ, Francioli LC, Tiao G, et al. The mutational constraint spectrum quantified from variation in 141,456 humans. Nature. 2020;581:434-43.

30. Li CH, Zhang Q, Teng B, Mustafa SJ, Huang JY, Yu HG. Src tyrosine kinase alters gating of hyperpolarization-activated HCN4 pacemaker channel through Tyr531. Am J Physiol Cell Physiol. 2008;294:C355–62.

31. Yu H, Chang F, Cohen IS. Pacemaker current exists in ventricular myocytes. Circ Res. 1993;72(1):232–6.

32. Garny A, Hunter PJ. OpenCOR: a modular and interoperable approach to computational biology. Front Physiol. 2015;6:1–2.

33. Severi S, Fantini M, Charawi LA, DiFrancesco D. An updated computational model of rabbit sinoatrial action potential to investigate the mechanisms of heart rate modulation. J Physiol. 2012;590:4483–99.

34. Seifert R, Scholten A, Gauss R, Mincheva A, Lichter P, Kaupp UB. Molecular characterization of a slowly gating human hyperpolarization-activated channel predominantly expressed in thalamus, heart, and testis. Proc Natl Acad Sci USA. 1999;96:9391–6.

35. Wang J, Al-Ouran R, Hu Y, Kim S-Y, Wan Y-W, Wangler MF, et al. MARRVEL: integration of human and model organism genetic resources to facilitate functional annotation of the human genome. Am J Hum Genet. 2017;100:843–53.

36. Adzhubei IA, Schmidt S, Peshkin L, Ramensky VE, Gerasimova A, Bork P, et al. A method and server for predicting damaging missense mutations. Nat Methods 2010;7(4):248–9.

37. Vaser R, Adusumalli S, Leng SN, Sikic M, Ng PC. SIFT missense predictions for genomes. Nat Protoc. 2016;11(1):1–9.

38. Kumar P, Henikoff S, Ng PC. Predicting the effects of coding nonsynonymous variants on protein function using the SIFT algorithm. Nat Protoc 2009;4:1073–81.

39. Baig SM, Koschak A, Lieb A, Gebhart M, Dafinger C, Nürnberg G, et al. Loss of Ca(v)1.3 (CACNA1D) function in a human channelopathy with bradycardia and congenital deafness. Nat Neurosci 2011;14(1):77–84.

40. Lei M, Zhang H, Grace AA, Huang CLH. SCN5A and sinoatrial node pacemaker function. Cardiovasc. Res. 2007;74:356–65.

41. Wilders R. Sinus bradycardia in carriers of the SCN5A-1795insD mutation: unraveling the mechanism through computer simulations. Int J Mol Sci. 2018;19(2):634.

42. Ye D, Tester DJ, Zhou W, Papagiannis J, Ackerman MJ. A pore-localizing CACNA1C-E1115K missense mutation, identified in a patient with idiopathic QT prolongation, bradycardia, and autism spectrum disorder, converts the L-type calcium channel into a hybrid nonselective monovalent cation channel. Heart Rhythm. 2019;16:270–8.

43. Ishikawa T, Tsuji Y, Makita N. Inherited bradyarrhythmia: a diverse genetic background. J Arrhythm. 2016;32:352–8.

44. Yu H, Wu J, Potapova I, Wymore RT, Holmes B, Zuckerman J, et al. MinK-related peptide 1: a beta subunit for the HCN ion channel subunit family enhances expression and speeds activation. Circ Res. 2001;88:E84–7.

45. BoSmith RE, Briggs I, Sturgess NC. Inhibitory actions of ZENECA ZD7288 on whole-cell hyperpolarization activated inward current (I_f) in guinea-pig dissociated sinoatrial node cells. Br J Pharmacol. 1993;110(1):343–9.

46. Marini C, Porro A, Rastetter A, et al. HCN1 mutation spectrum: from neonatal epileptic encephalopathy to benign generalized epilepsy and beyond. Brain. 2018;141:3160–78.

47. DiFrancesco JC, Barbuti A, Milanesi R, Coco S, Bucchi A, Bottelli G, et al. Recessive loss-of-function mutation in the pacemaker HCN2 channel causing increased neuronal excitability in a patient with idiopathic generalized epilepsy. J Neurosci. 2011;31:17327–37.

48. Nykamp K, Anderson M, Powers M, Garcia J, Herrera B, Ho Y-Y, et al. Sherloc: a comprehensive refinement of the ACMG–AMP variant classification criteria. Genet Med. 2017;19(10):1105–17. https://doi.org/10.1038/gim.2017.37

49. Verkerk AO, Wilders R, van Borren MM, Peters RJ, Broekhuis E, Lam K, et al. Pacemaker current (I_f) in the human sinoatrial node. Eur Heart J. 2007;28(20):2472–8.

SUPPORTING INFORMATION

Additional supporting information may be found online in the Supporting Information section.